Particles II

Access the latest eBook →

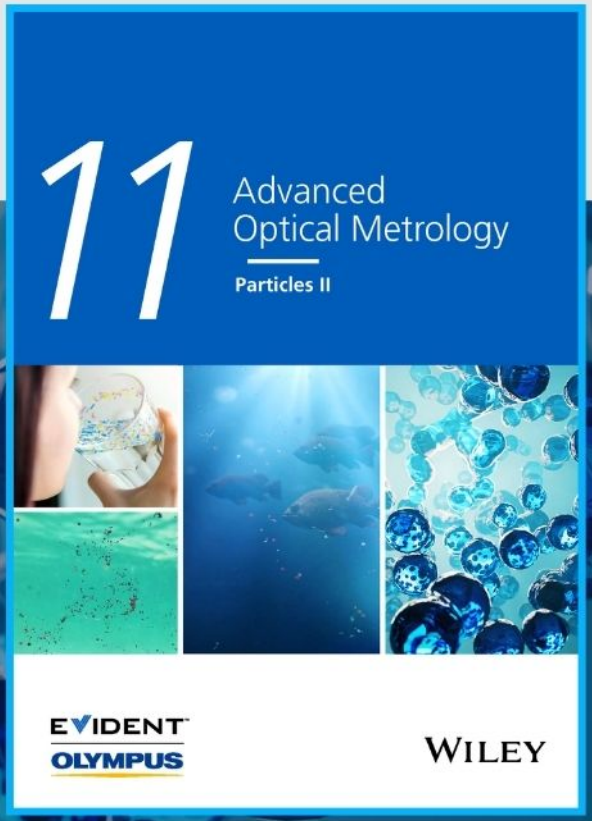

Impact on Biological Systems and the Environment

This eBook is dedicated to the research of Professor David Wertheim.
In collaboration with various groups, Professor Wertheim uses confocal microscopy to analyse the impact of different types of particles on human health and the environment, with a focus on human health-hazardous particles detected with solid-state nuclear track detectors (SSNTD). Download for free, today.

EVIDENT
OLYMPUS

WILEY

ADVANCED MATERIALS
www.advmat.de

Reduced Intrinsic Non-Radiative Losses Allow Room-Temperature Triplet Emission from Purely Organic Emitters

Yungui Li, Lihui Jiang, Wenlan Liu, Shunqi Xu, Tian-Yi Li, Felix Fries, Olaf Zeika, Yingping Zou, Charusheela Ramanan, Simone Lenk, Reinhard Scholz, Denis Andrienko, Xinliang Feng, Karl Leo, and Sebastian Reineke**

Persistent luminescence from triplet excitons in organic molecules is rare, as fast non-radiative deactivation typically dominates over radiative transitions. This work demonstrates that the substitution of a hydrogen atom in a derivative of phenanthroimidazole with an *N*-phenyl ring can substantially stabilize the excited state. This stabilization converts an organic material without phosphorescence emission into a molecular system exhibiting efficient and ultralong afterglow phosphorescence at room temperature. Results from systematic photophysical investigations, kinetic modeling, excited-state dynamic modeling, and single-crystal structure analysis identify that the long-lived triplets originate from a reduction of intrinsic non-radiative molecular relaxations. Further modification of the *N*-phenyl ring with halogen atoms affects the afterglow lifetime and quantum yield. As a proof-of-concept, an anticounterfeiting device is demonstrated with a time-dependent Morse code feature for data encryption based on these emitters. A fundamental design principle is outlined to achieve long-lived and emissive triplet states by suppressing intrinsic non-radiative relaxations in the form of molecular vibrations or rotations.

1. Introduction

Phosphorescent materials with triplet emission have been widely used for organic light-emitting diodes (OLEDs) to fully harvest triplets under electrical excitation.[1,2] However, metal components, such as copper, iridium, and europium, are normally needed to enhance the intersystem crossing (ISC) and the subsequent triplet radiative transition but are associated with potential environmental hazards and increased cost.[3,4] Purely organic materials that exhibit ultralong room-temperature phosphorescence (URTP) with emission lifetimes on the order of a second have recently received considerable attention. These materials possess fascinating features, such as transparency, flexibility, long persistence, and versatile molecular designs. They have been used in various applications, such as programmable tags, afterglow OLEDs, bioimaging devices, and emission-based sensors.[5–13]

Phosphorescence, i.e., the luminescence originating from molecular triplet states, is often weak or not observed at all because the spin flip required for this process is quantum mechanically "transition" forbidden in the absence of a coupling mechanism. Consequently, direct photoexcitation to the triplet state is often not allowed. Rather, triplet states are generated in a two-step process involving photoexcitation to a singlet state and subsequent ISC. The latter also involves a spin flip, which also requires effective coupling. The ISC process competes with direct deactivation mechanisms from the singlet state, including both non-radiative relaxations as well as radiative decay (fluorescence).[14] Spin–orbit and/or vibrational coupling often facilitate the spin-flip process, thus generating and deactivating triplet states in organic molecules. Without strong spin–orbital coupling usually introduced by

Dr. Y. Li,[+] Prof. L. Jiang, Dr. T.-Y. Li, F. Fries, Dr. O. Zeika, Dr. S. Lenk, Prof. K. Leo, Prof. S. Reineke
Dresden Integrated Center for Applied Physics and Photonic Materials (IAPP) and Institute for Applied Physics
Technische Universität Dresden
Nöthnitzer Straße 61, 01062 Dresden, Germany
E-mail: sebastian.reineke@tu-dresden.de

The ORCID identification number(s) for the author(s) of this article can be found under https://doi.org/10.1002/adma.202101844.

© 2021 The Authors. Advanced Materials published by Wiley-VCH GmbH. This is an open access article under the terms of the Creative Commons Attribution-NonCommercial License, which permits use, distribution and reproduction in any medium, provided the original work is properly cited and is not used for commercial purposes.

[+]Present address: Max Planck Institute for Polymer Research, Ackermannweg 10, 55128 Mainz, Germany

Prof. L. Jiang, Prof. Y. Zou
College of Chemistry and Chemical Engineering
Central South University
Changsha 410083, China
E-mail: jianglh@csu.edu.cn

Dr. W. Liu, Dr. C. Ramanan, Dr. D. Andrienko
Max Planck Institute for Polymer Research
Ackermannweg 10, 55128 Mainz, Germany

Dr. S. Xu, Prof. X. Feng
Center for Advancing Electronics Dresden (cfaed) and Department of Chemistry and Food Chemistry
Technische Universität Dresden
Mommsenstraße 4, 01069 Dresden, Germany

Dr. R. Scholz
Leibniz-Institut für Polymerforschung Dresden e.V.
01069 Dresden, Germany

DOI: 10.1002/adma.202101844

heavy metal atoms,[14,15] the overall radiative transition from the triplet state is still unstable and thus prone to internal and external quenching processes. Consequently, the low radiative rate can lead to very long emission lifetimes τ_P if loss channels are suppressed.[16,17]

Long-lived triplets can be easily quenched via intermolecular collision or energy transfer to oxygen, making it difficult to observe from purely organic materials at room temperature under ambient conditions.[18] Strategies making use of El-Sayed's rule, the heavy atom effect and resonance-activated spin-flipping have been demonstrated to successfully facilitate the ISC process.[17,19–21] Furthermore, methodologies such as crystal engineering, the use of oxygen barrier materials and external rigid confinement by polymer matrices have been applied to reduce the non-radiative deactivation of triplet states via collisions, molecular motion, or energy transfer loss.[13,22,23] Investigations of the well-known URTP emitter tetra-*N*-phenylbenzidine (TPD) and small-molecule fragments of TPD have shown that compounds containing a biphenyl core can exhibit URTP emission.[24] However, there is still limited understanding of the origin of triplet emission from purely organic emitters. Clearly, further investigations of the relationship between the molecular structure and the ability to exhibit URTP are needed. Here, we present results indicating that a group of phenanthroimidazole derivatives possess different photophysical properties—with or without URTP—although the only difference in molecular structure is the presence or absence of an *N*-phenyl ring.

2. Results and Discussion

2.1. Photophysical Properties

A series of phenanthroimidazole derivatives were obtained in high yield (70–92%) by a one-step Debus-Radziszewski reaction from commercially available materials. The molecular structures are shown in **Figure 1**a. The synthesis procedure and structure characterization are described in the Supporting Information. The molecules are named as 4-(1-phenyl-1*H*-phenanthro[9,10-*d*]imidazol-2-yl)-*N*,*N*-di-*p*-tolylbenzenamine (TPMN), 4-(1-(4-fluorophenyl)-1*H*-phenanthro[9,10-*d*]imidazol-2-yl)-*N*,*N*-di-*p*-tolylbenzenamine (TPMF), 4-(1-(4-chlorophenyl)-1*H*-phenanthro[9,10-*d*]imidazol-2-yl)-*N*,*N*-di-*p*-tolylbenzenamine (TPMCl), 4-(1-(4-bromophenyl)-1*H*-phenanthro[9,10-*d*]imidazol-2-yl)-*N*,*N*-di-*p*-tolylbenzenamine (TPMBr), 4-(1-(4-iodophenyl)-1*H*-phenanthro[9,10-*d*]imidazol-2-yl)-*N*,*N*-di-*p*-tolylbenzenamine (TPMI), and 4-(1*H*-phenanthro[9,10-*d*]imidazol-2-yl)-*N*,*N*-di-*p*-tolylbenzenamine (TPN). When these materials were mixed with a rigid poly(methyl methacrylate) (PMMA) matrix and sealed with a layer of Exceval as an oxygen barrier,[13] URTP emission was observed after the cessation of UV excitation for all molecules in the TPMX series except TPN, as shown in Figure 1b. Further systematic studies were conducted to explore the different photophysical factors between TPN and the TPMX series that influence the URTP.

The UV–Vis absorption characteristics were similar for all materials, as shown in **Figure 2**a. The absorption bands in the range of 365 to 370 nm were assigned to the $\pi \rightarrow \pi^*$ transition of the phenanthroimidazole ring.[25] The onset of TPN absorption was shifted to a slightly higher energy than that of the TPMX series because of the slightly longer conjugation of the TPMX series. The low absorption in the deep-blue region made the spin-coated films transparent under white light illumination, as shown in Figure 1b. Meanwhile, the absorption of blue light also makes it possible to excite these emitters with visible light. A broad photoluminescence (PL) spectrum with blue emission in dichloromethane was observed for these molecules (Figure S14, Support ing Information).

As presented in Figure 2b, at a concentration of 2 wt% in the PMMA matrix, the steady-state fluorescence spectrum of TPN was slightly blueshifted compared to that of the TPMX series with an *N*-phenyl moiety. The fluorescence peak of TPMN was observed at 426 nm, while for TPN, the emission peak was at 421 nm. Line shape analysis of the fluorescence spectra demonstrated that the fundamental transition energies E_{00} from S_1 to

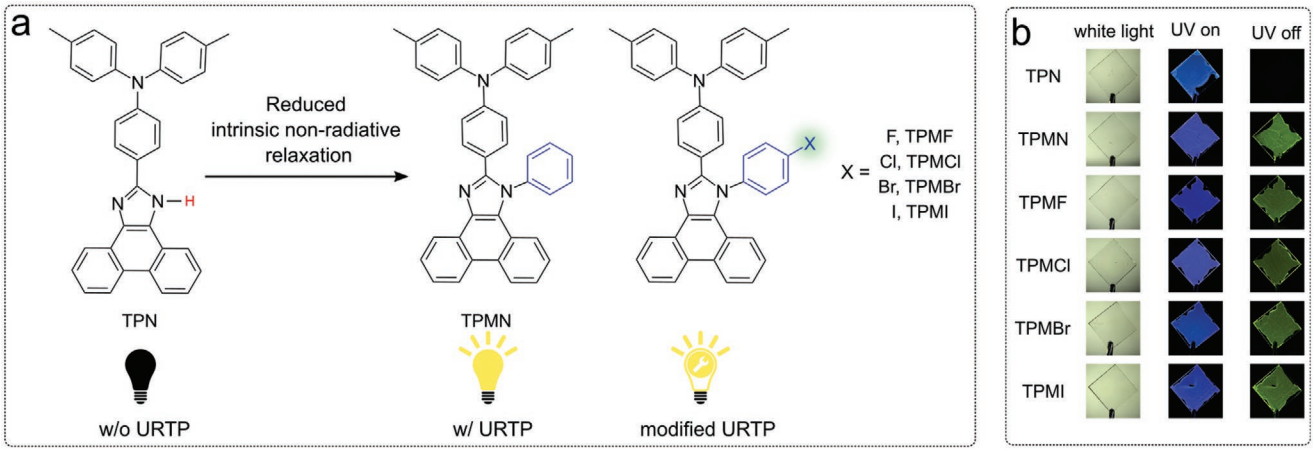

Figure 1. Chemical structures and a schematic presentation of URTP emission. a) Chemical structures of the phenanthroimidazole derivatives investigated. The difference between the TPMX series and TPN is merely the presence of the *N*-phenyl ring attached to the imidazole group. b) Pictures for the investigated emitters under UV excitation and the delayed emission after the stop of UV excitation, taken at room temperature. Samples are sealed with O_2 barrier. There is no delayed emission for TPN while prominent delayed emission can be observed for the TPMX series.

© 2021 The Authors. Advanced Materials published by Wiley-VCH GmbH

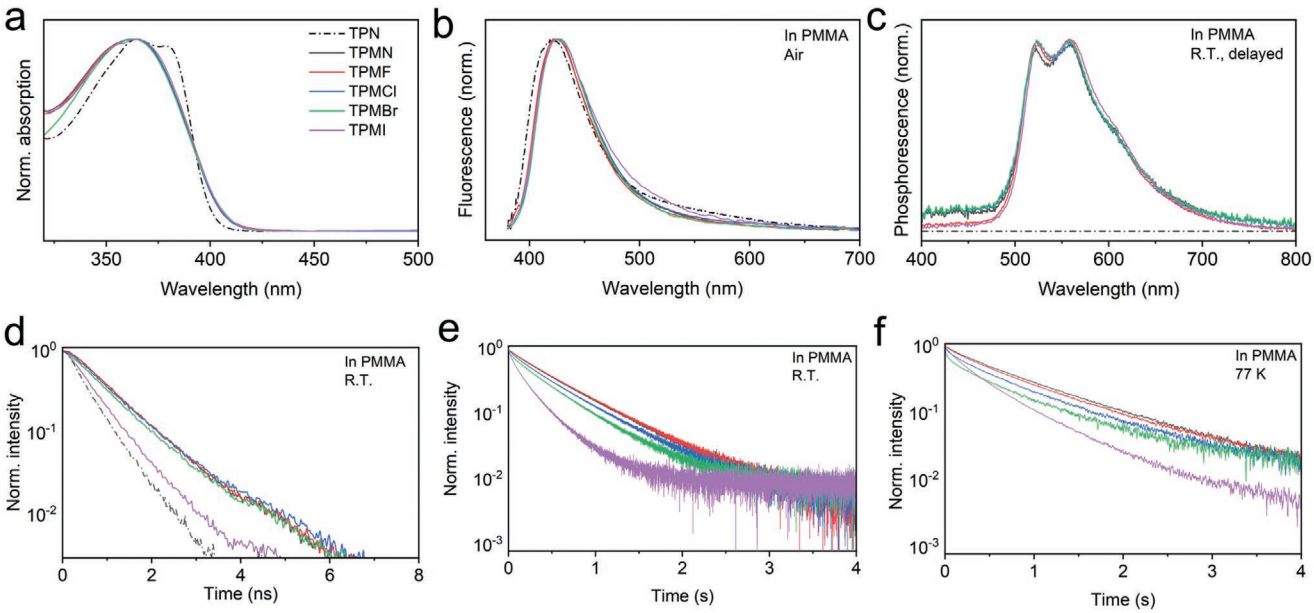

Figure 2. Photophysical properties. a) UV–vis absorption in dichloromethane. For (b–f) emitters are buried in a PMMA host at a concentration of 2 wt%. b) Steady-state emission in air. c) Spectra of delayed emission at room temperature. d) Fluorescence transients in ambient atmosphere at room temperature by a 373 nm laser. e) Decay of the phosphorescence emission at room temperature in N_2. f) Decay of the phosphorescence in liquid nitrogen (77 K). The excitation source for (b), (c), (e), and (f) is a UV-LED with the wavelength centered at 365 nm.

S_0 (Figure S15 and Table S1, Supporting Information) were very similar for TPN and TPMN, indicating that the *N*-phenyl ring of TPMX is only partially conjugated with the phenanthroimidazole plane.

Additional photophysical measurements indicated the occurrence of delayed green-yellow emission at room temperature for the TPMX series in the PMMA matrix. Emitters were purified by vacuum sublimation before sample fabrication to avoid artifacts due to impurities.[26] The delayed emission could be quenched completely by exposure to air, suggesting the interaction of triplet states with molecular oxygen.[13] The possibility of thermally activated delayed fluorescence can be ruled out because of the large singlet-triplet splitting ΔE_{ST}.[27–29] According to the line shape analysis (Figure S14 and Table S1, Supporting Information),[30,31] the materials possess a substantial ΔE_{ST} (≈400 meV), indicating that reverse ISC (RISC) is very weak. The delayed spectra in a nitrogen atmosphere at room temperature (Figure 2c) and the phosphorescence spectra in liquid nitrogen (Figure S14, Supporting Information) agree very well, allowing assignment of the afterglow at room temperature as URTP.

The fluorescence decays of all the materials are shown in Figure 2d. Almost identical fluorescence decay profiles were observed for TPMN, TPMF, TPMCl, and TPMBr, with lifetimes of ≈0.9 ns, while the fluorescence decay of TPMI was faster (≈0.7 ns). Among all these emitters, TPN exhibited the fastest decay with the shortest singlet lifetime of ≈0.5 ns. The fluorescence lifetimes τ_F of all the investigated emitters are summarized in **Table 1**, and the fitting is presented in Figure S18 and Table S4 (Supporting Information).

The URTP decay profiles of the TPMX series in PMMA are presented in Figure 2e, and the respective decay lifetimes τ_P of the URTP are summarized in Table 1. The fitting details are shown in Figure S16 and Table S2 (Supporting Information). TPMN exhibits an afterglow for up to several seconds, with a τ_P as long as 0.58 s, and TPMF possesses a similar τ_P (0.59 s). The

Table 1. Summary of the photophysical properties.

Emitter[a)]	τ_F [ns]	τ_P [ms] @ R.T.	τ_P [ms] @ 77 K	Φ_F [%]	Φ_P [%][b)]	$k_{r,F}$ ($\times 10^8$ s^{-1})	$k_{nr,P}$ ($\times$s^{-1})[c)]	$k_{nr,F}$ ($\times 10^8$ s^{-1})[e)]
TPN	0.52	–	–	24.9	–	4.79	[d)]	14.12
TPMN	0.94	576.4	945.5	57.4	3.0	6.07	1.61	4.19
TPMF	0.97	589.2	910.4	56.2	1.1	5.78	1.65	4.39
TPMCl	0.98	529.3	826.2	56.0	2.9	5.68	1.76	4.17
TPMBr	0.94	453.7	723.7	54.9	3.9	5.86	2.01	4.39
TPMI	0.68	265.9	534.0	27.2	5.5	4.01	3.48	9.93

[a)]Films spin-coated with organic emitters in PMMA with a concentration of 2 wt%; [b)]Measured at room-temperature in nitrogen atmosphere; [c)]Based on the assumption in Case 1 ($k_{nr,F} = 0$ and $\Phi_{nr,F} = 0$). Details in Table S5 (Supporting Information); [d)]The rate $k_{nr,P}$ for TPN is orders higher than $k_{r,P}$ or $k_{nr,P}$ for TPMN, as explained in Supporting Information; [e)]Based on the assumption in Case 2 ($k_{nr,P} = 0$ and $\Phi_{nr,P} = 0$). Details in Table S6 (Supporting Information).

© 2021 The Authors. Advanced Materials published by Wiley-VCH GmbH

lifetimes τ_P of TPMCl (0.53 s) and TPMBr (0.46 s) are slightly shorter than that of TPMN. The URTP lifetime τ_P of TPMI is 0.26 s. In contrast, no phosphorescence could be observed for TPN (cf. Figure 2c).

For the TPMX series, the phosphorescence decay was slowed down in liquid nitrogen at 77 K, where the detailed lifetimes are presented in Figure 2f and Table 1. The fitting details are provided in Figure S17 and Table S3 (Supporting Information). Compared to the τ_P at room temperature, it extends to 0.94 s for TPMN, 0.91 s for TPMF, 0.83 s for TPMCl, 0.72 s for TPMBr, and 0.54 s for TPMI. The significant difference in τ_P at different temperatures indicates that non-radiative relaxation from the triplet state T_1 to S_0 occurs at room temperature for the TPMX series, since the intrinsic non-radiative processes are temperature-dependent.[32,33] From TPMF to TPMI, the lifetime τ_P becomes shorter as the atomic number increases. On the other hand, no phosphorescence was detected for TPN in liquid nitrogen. Further time-resolved photoluminescence spectral investigations performed by means of a streak camera at 50 or 10 K indicated that there was no clear phosphorescence emission after excitation within approximately 1 ms, as shown in Figure S15 (Supporting Information).

The absolute photoluminescence quantum yields (PLQYs) of fluorescence Φ_F and phosphorescence Φ_P at room temperature were detected in a calibrated integrating sphere, and the results are summarized in Table 1. A moderate Φ_F of 24.9% for TPN indicates that ≈75% of singlet states were deactivated through the following possible non-radiative processes: 1) via ISC to triplet states followed by non-radiative deactivation to S_0; 2) depopulation to S_0 directly from the singlet state. The quantum yield Φ_F was ≈55–58% for TPMN, TPMF, TPMCl, and TPMBr. Φ_P was ≈3.0% for TPMN, TPMCl, and TPMBr and 1.1% for TPMF. TPMI showed a higher Φ_P of 5.5% and a Φ_F of 27.2%.

2.2. Origin of URTP from TPN to TPMN

Theoretically, the rate k_{ISC} from the S_1 state to the T_m state is dependent on the spin–orbit interaction between S_1 and T_m:[14,15]

$$k_{ISC,m} \propto \frac{2\pi}{\hbar}\xi^2 = \frac{2\pi}{\hbar}\left\langle \Psi_1^{1(0)} \middle| H_{SO} \middle| \Psi_m^{3(0)} \right\rangle \tag{1}$$

where ξ is spin–orbit coupling (SOC) factors, $\Psi_m^{3(0)}$ the electronic wave function of the zeroth vibrational level of the m-th order triplet state (T_m), in which the spin–orbit Hamiltonian H_{SO} can be written as follows:[14,15]

$$H_{SO} = \alpha_F^2 \sum_{\mu}^{N}\sum_{i}^{n} \frac{Z_\mu}{r_{i\mu}^3}\overrightarrow{L_i}\cdot\overrightarrow{S_i} \tag{2}$$

where α_F denotes the fine-structure constant, Z represents the effective nuclear charge at the nucleus μ, and S and L are the spin and orbital angular momenta of electron i.

According to Equations 1 and 2, the spin–orbit Hamiltonian H_{SO} and the rate k_{ISC} can be enhanced by increasing the nuclear charge. However, TPN and TPMN do not include any heavy atoms to enhance the spin–orbit coupling. As shown in **Figure 3**a,c, for TPN and TPMN, the simulated SOC factors ξ between the S_1 and triplet states T_2 and T_1, which are lower in energy than S_1, are very similar. Comparable SOC factors indicate a similar spin-flip rate from the singlet state to the triplet state for TPN and TPMN. Furthermore, similar ξ factors have been obtained for TPN and TPMN between T_1 and S_0, demonstrating that these complexes possess similar radiative couplings from the triplet state to the ground state as well. It is worth noting that these SOC factors are in accordance with other reports for purely organic URTP emitters with different chemical composition.[20,34] Even though the SOC values are low for the emitters investigated, it is important that the SOC is nonzero, which renders the singlet–triplet state conversion possible, so that both ISC and phosphorescence can occur. In contrary to other use cases for luminophores where fast radiative decay is desired, the low triplet radiation rate gives rise to a long triplet emission lifetime. In other words, low SOC factors make long triplet emission possible, which is of vital importance for URTP emitters with long afterglow, where the remaining task is to effectively suppress non-radiative relaxations. Based on these calculated results, the differences in phosphorescence between TPN and TPMN must have a different origin, which we will discuss later. As shown in Figure 3a,c and Figure S21 (Supporting Information), similar oscillator strengths f for S_1 can be obtained for all investigated emitters, indicating that the intrinsic radiative rate of the singlet state is comparable for all emitters.[14,35]

The characteristics of the excited states can be analyzed in terms of the natural transition orbitals (NTOs). As shown in Figure 3b,d, the transitions from hole to electron NTOs for TPN and TPMN are dominant, with proportions close to 90%. The hole and electron NTOs of the TPN and TPMN singlet states both extend to the donor benzenamine group and the acceptor phenanthroimidazole moiety, while the electron NTO of TPMN partially extends to the *N*-phenyl ring as well. For the triplet states, the difference between T_1 for TPN and TPMN is mainly the *N*-phenyl ring and the benzenamine group, while a major difference for T_2 can be noted in the acceptor phenanthroimidazole moiety, as shown in Figure 3b,d and Figure S20 (Supporting Information).

To gain deeper insight into the origin of the URTP for the TPMX series, kinetic modeling was performed to quantitatively investigate the rates of the processes involved based on the experimental photophysical results. As shown in Figure 3e, kinetically, there are several requirements for achieving efficient URTP from purely organic emitters: 1) a high ISC rate k_{ISC}, which competes with the radiative rate of singlet states $k_{r,F}$ and the non-radiative rate $k_{nr,F}$, to generate a considerable number of triplet states and 2) a high or at least comparable radiative rate of triplet states $k_{r,P}$ relative to the non-radiative rate $k_{nr,P}$ or the triplet quenching rate $k_{q,P}$.[14] From a theoretical perspective, the non-radiative deactivation from a singlet state ($\Phi_{nr,F}$) or a triplet state ($\Phi_{nr,P}$) can contribute to the energy loss:

$$\Phi_F + \Phi_P + \Phi_{nr,P} + \Phi_{nr,F} = 1 \tag{3}$$

where Φ_F and Φ_P are the absolute PLQYs of fluorescence and phosphorescence, respectively. The fluorescence quantum efficiency Φ_F is kinetically determined by the following equation:

© 2021 The Authors. Advanced Materials published by Wiley-VCH GmbH

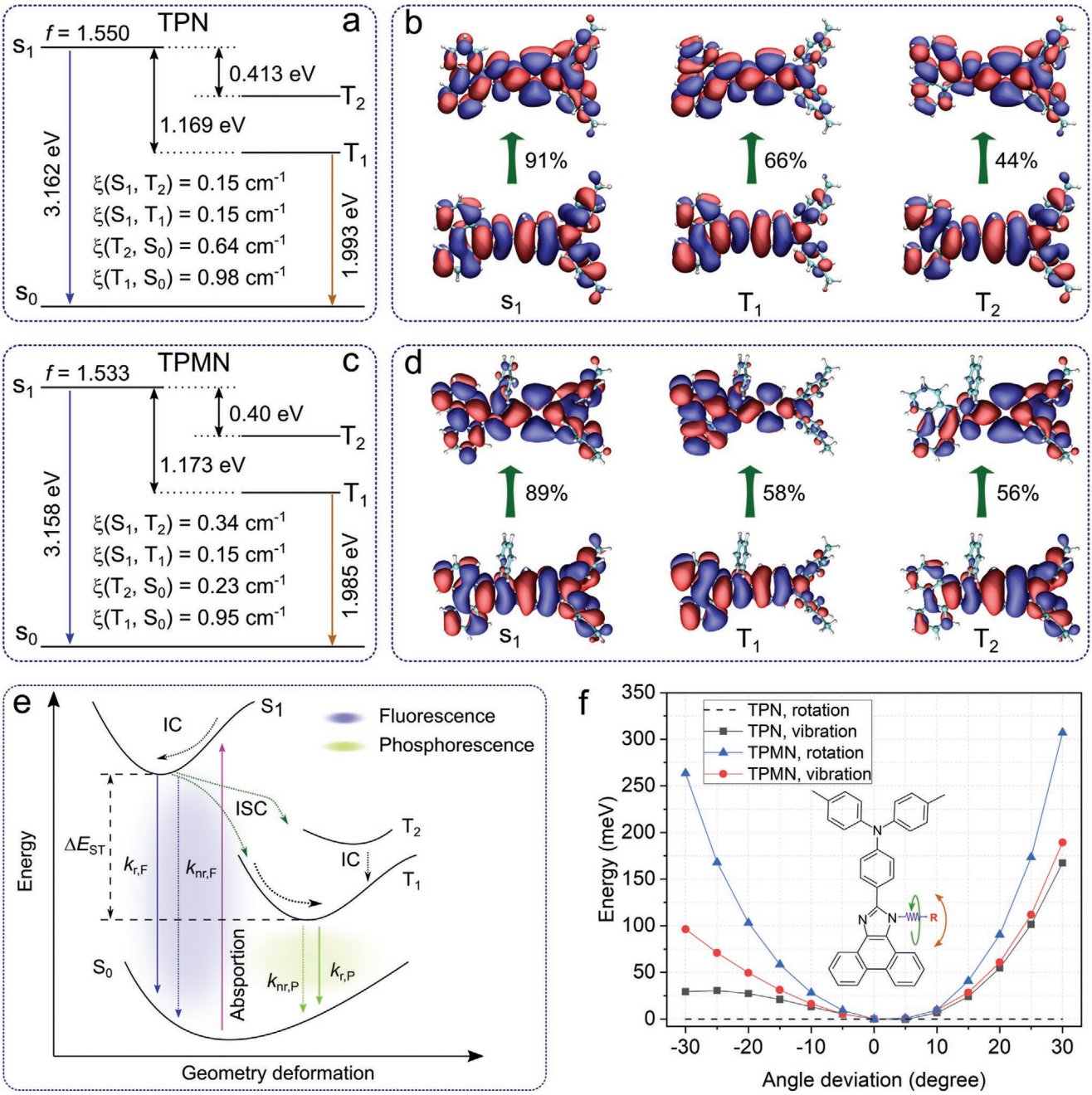

Figure 3. Theoretical investigation on the origin of URTP emission. a,c) Simulated energy diagrams, the oscillator strength f of the S_1 state, SOC factors ξ between singlet and triplet states below S_1 of TPN (a) and TPMN (c). b,d) The major natural transition orbitals (hole ones at the bottom and particle ones on the top) and the corresponding proportions for TPN (b) and TPMN (d). e) Schematic illustration about URTP mechanism. f) Simulated energy barrier as a function of the molecular vibration or rotation angles for TPN and TPMN. The inset is a schematic presentation of the out-of-plane vibration, rotation, or stretching of the group R (hydrogen for TPN and *N*-phenyl ring for TPMN).

$$\Phi_F = \frac{k_{r,F}}{k_{r,F} + k_{nr,F} + k_{ISC}} = k_{r,F} \cdot \tau_F \quad (4)$$

The ISC quantum yield Φ_{ISC} is determined by the following equation:

$$\Phi_{ISC} = k_{ISC} \cdot \tau_F \quad (5)$$

Without considering k_{RISC} because of the large ΔE_{ST}, the lifetime of triplet states τ_P can be described as follows:

$$\tau_P = \frac{1}{k_{r,P} + k_{nr,P} + k_{q,P}} \quad (6)$$

where $k_{r,P}$ is the radiative rate of phosphorescence, $k_{nr,P}$ is the intrinsic non-radiative rate of phosphorescence and $k_{q,P}$ is the

© 2021 The Authors. Advanced Materials published by Wiley-VCH GmbH

triplet quenching rate. In this study, emitters are dispersed in a rigid matrix with a low concentration of 2 wt%, while the quantum yield Φ_P is measured under low UV excitation in a nitrogen atmosphere. The excitation dose is low, so singlet–triplet annihilation or triplet-triplet annihilation can be excluded. The quenching effect from oxygen and intermolecular annihilation/collision at a low emitter concentration can also be reasonably eliminated, yielding the quenching rate $k_{q,P} \approx 0$. Furthermore, the quantum yield of phosphorescence emission Φ_P can be expressed as follows:

$$\Phi_P = \Phi_{ISC} \cdot k_{r,P} \cdot \tau_P \tag{7}$$

Thus, the depopulation of triplet states results from intrinsic non-radiative relaxation or radiation. However, since non-radiative relaxation is a dark process, there is no direct access to the intrinsic non-radiative rates from singlet states $k_{nr,F}$ or triplet states $k_{nr,P}$. We here consider two extreme situations: in case 1, non-radiative losses result only from triplet states, giving $k_{nr,F} = 0$ and $\Phi_{nr,F} = 0$; in case 2, non-radiative losses come only from singlet states, giving $k_{nr,P} = 0$ and $\Phi_{nr,P} = 0$. Realistically, it is reasonable that the actual kinetic rates for the TPMX series fall in between these two extreme cases for the following reasons: i) Experimentally, the different phosphorescence decay profiles for the TPMX series at room temperature (Figure 2e) and 77 K (Figure 2f) indicate that there are non-radiative losses from triplet states at room temperature.[23] Thus, the rates k_{ISC} and $k_{nr,P}$ for the TPMX series should be higher than calculated rates in case 2 ($k_{nr,P} = 0$). ii) Since the non-radiative loss from singlet states is universal for conventional fluorescent emitters, the rates k_{ISC} and $k_{nr,P}$ of TPMX should be smaller than that in case 1 ($k_{nr,F} = 0$).[36–38] Nevertheless, in the following, we will discuss these two cases to explain the photophysical observations between TPN and TPMN on a quantitative level.

For each of the cases, the remaining kinetic rates for the TPMX series can be calculated based on the experimental photophysical results obtained at room temperature. For TPN, which is the only material to show no URTP, a comparison of the density functional theory (DFT) simulation results allows us to assume that k_{ISC} is similar for TPN and TPMN. Then, all other kinetic rates for TPN can be estimated, according to Equations 2–7. The detailed modeling for each case is shown in Supporting Information.

As summarized in Table 1, Tables S5 and S6 (Supporting Information), the rates $k_{r,P}$ and $k_{nr,P}$ for TPMN are on the order of 1 s^{-1},[39] except for case 2, where $k_{nr,P}$ is set to 0. However, according to Equations 6 and 7, based on the experimental result of $\Phi_{r,P} = 0$ for TPN, the non-radiative rate $k_{nr,P}$ for TPN should be orders of magnitude higher. Thus, kinetically, the generated triplet states of TPN are deactivated much faster via non-radiative processes than those of TPMN. Furthermore, in both cases, the non-radiative decay rates of singlet states $k_{nr,F}$ of TPN are higher than those of TPMN. Despite the uncertainty of the actual rates, we can conclude in any case that the presence of the *N*-phenyl ring in the TPMX series definitely reduces the non-radiative losses from singlet or triplet states compared to those of TPN.

To clarify the molecular origin of pronounced non-radiative decay in TPN, we performed DFT calculations of the excited states of TPN and TPMN. As shown in Figure S23 (Supporting Information), for emitters in the geometry-optimized triplet state, the movement of the hydrogen atom attached to the imidazole ring of TPN occurs at a low-frequency range, similar to that of conventional fluorescence emitters.[36] The frequencies of the vibration of the hydrogen atom in the out-of-plane direction are 296.4 and 447.1 cm^{-1}, while the in-plane vibration is generally coupled with the movements of other moieties, such as donor or acceptor plane vibrations, with frequencies of 1365, 1380, 1624, and 1632 cm^{-1}. The stretching mode of the hydrogen atom has a frequency of 3706.5 cm^{-1}. For TPMN, the *N*-phenyl ring vibration/rotation modes are mainly located at 833.8, 1032, and 1663 cm^{-1}. From normal mode analysis, it is possible to estimate the energy needed for exciting a vibration of the hydrogen in the imidazole ring for TPN, or a vibration or rotation of the *N*-phenyl ring for TPMN. For the hydrogen atom which is attached in the imidazole ring in TPN, the energy needed for the rotation movement along the bond is negligible. As shown in Figure 3f, only 29.4 meV is needed to displace the hydrogen atom by an angle of −30° from the optimized T_1 configuration. Therefore, this motion can be activated thermally at room temperature, leading to pronounced non-radiative losses for the triplet state.[36–38] However, 96.3 meV is required to displace the *N*-phenyl ring by −30° from the configuration with the minimum energy. Furthermore, an even higher energy barrier of 263.5 meV is expected for rotation of the *N*-phenyl ring by −30° from the optimized T_1 configuration. An even higher energy barrier is observed for vibrating/rotating in another direction. The asymmetric energy barrier for different vibration/rotation directions is likely due to the relative spatial arrangement of the donor moiety and the acceptor in the molecular configuration with the minimum potential. As shown in Figure S24 (Supporting Information), when considering the rotation of benzene rings in the triphenylamine group, the corresponding potential energy has very similar shape and energy barriers in TPN and TPMN. Further, the rotation of benzene rings has a higher energy barrier compared to that of a vibration of a hydrogen atom in TPN (Figure 3f). This allows us to conclude that the difference in the rotational and vibrational spectra caused by the remaining part of the two molecules can only affect the non-radiative transition as a secondary effect. The low energy barrier for the substantial out-of-plane motion of the hydrogen atom in the imidazole ring may explain the lack of room-temperature phosphorescence emission in TPN.

It is interesting whether other substitution groups can have similar effects. To investigate such influences, we carried out molecular simulations for TPN substituted with an *N*-methyl group attached to the imidazole ring, named as TPN-CH_3 in the following discussion. As shown in Figure S25 (Supporting Information), the singlet and triplet energy levels for TPN-CH_3 is very close to that of TPN and TPMN, which is shown in Figure 3a,c. The SOC factors are also comparable with that of TPN and TPMN, indicating that the possibility of triplet generation and radiation for TPN-CH_3 is expected to be similar to TPN and TPMN. The NTOs of the singlet and triplet states for TPN-CH_3 are shown in Figure S26 (Supporting Information). It shows that the *N*-methyl group contributes to the electron cloud distribution for both HOMO and LUMO orbitals, which is different from TPMN.

© 2021 The Authors. Advanced Materials published by Wiley-VCH GmbH

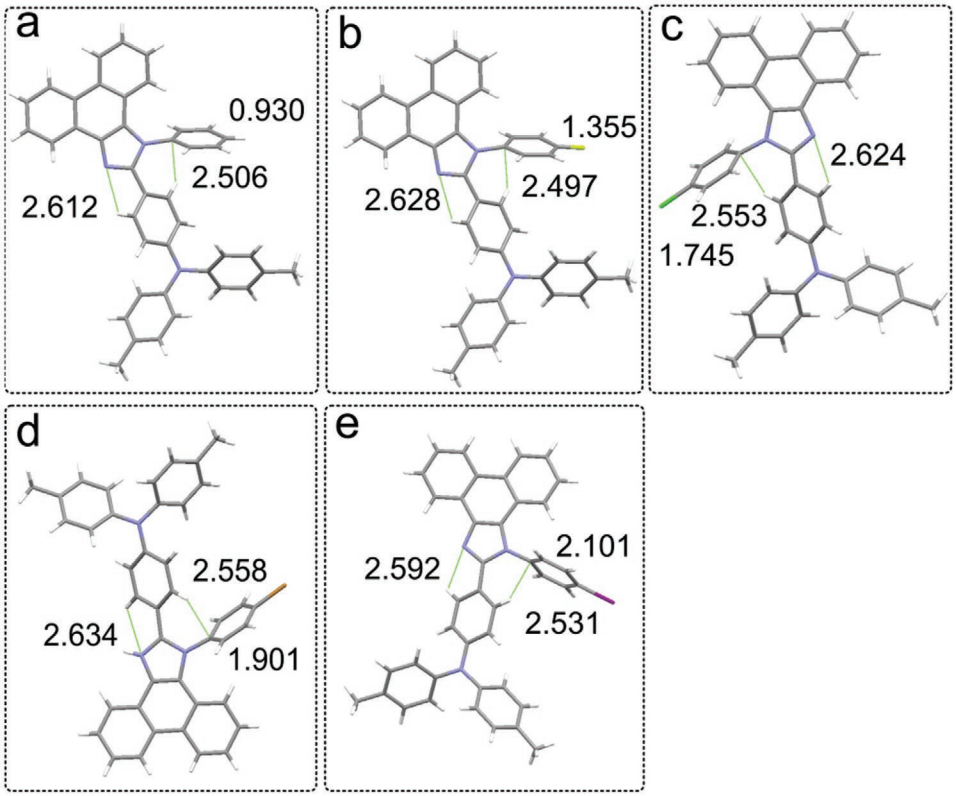

Figure 4. a–e) Effect of halogen atoms. Single-crystal structure for TPMN (a), TPMF (b), TPMCl (c), TPMBr (d), and TPMI (e). Single-crystal structures are observed from the *a*-axis. Selected distances are highlighted, in units of Ångström.

Further simulations on the *N*-methyl group vibration in TPN-CH_3 indicate that the energy barrier of methyl group vibration is much larger compared to that of the hydrogen atom vibration in TPN, as shown in Figure S27 (Supporting Information). Such a high energy barrier makes the non-radiative rate low in the forms of molecular vibrations. The energy barrier is even higher than that of the *N*-phenyl ring vibration in TPMN. The possible reason could be that the *N*-phenyl ring in TPMN is almost perpendicular with the phenanthro[9,10-*d*]imidazole ring, as shown in **Figure 4**a. The steric hindrance of the *N*-methyl group is larger than the *N*-phenyl ring when vibrating in the perpendicular direction of the phenanthro[9,10-*d*]imidazole ring. Further, the *N*-methyl group is conjugated with the imidazole ring, while the conjugation is broken for *N*-phenyl ring in TPMN, as shown in Figure S26 (Supporting Information). Here, one would expect a higher energy barrier of molecular vibration for a tightly bonded *N*-methyl group with conjugation to the π-system compared to a vertically orientated *N*-phenyl ring without π-conjugation. Considering these simulation results, it is possible that TPN molecules substituted with other groups such as an *N*-methyl group can also be potential URTP emitters.

2.3. Effect of Halogen Atoms

According to Equations 1, 2, and 7, Φ_{ISC} and Φ_P can be further increased by selecting atoms with high atomic numbers. Therefore, we have included a series of terminal halogen atoms to the *N*-phenyl ring to investigate, if this seemingly phosphorescence-sensitive part of the molecule can be further influenced—possibly to the better—by the heavy atom effect.[14,15] Experimentally, it should be noted that the trends of Φ_P and $k_{r,P}$ for TPMN, TPMF, and TPMCl are different from the typical heavy atom effect, as shown in Table 1, Tables S5 and S6 (Supporting Information). A possible reason for this finding is that the atomic number of chlorine is not large enough to significantly enhance ISC, while the difference in electron-withdrawing ability plays a more important role, tuning the geometry of these emitters via intramolecular interactions in a subtle and complicated manner.[22]

As shown in Figure 4a, the C—H bond length in the *N*-phenyl ring is 0.930 Å for the TPMN single crystal, while to the halogen-substituted bond lengths are 1.355 Å for the C—F bond (TPMF, Figure 4b), 1.745 Å for C-Cl (TPMCl, Figure 4c), 1.901 Å for C—Br (TPMBr, Figure 4d) and 2.101 Å for C—I (TPMI, Figure 4e). Weak intramolecular interactions can be observed within the single-crystal structure. Intramolecular hydrogen bonding in the form of C—H···N can be resolved, with distances of 2.612 Å for TPMN, 2.628 Å for TPMF, 2.624 Å for TPMCl, 2.634 Å for TPMBr and 2.592 Å for TPMI. The shortest C···H distance between a C atom of the *N*-phenyl ring (R1) and a H atom of the phenyl of amine (R2) is 2.506 Å for TPMN, 2.497 Å for TPMF, 2.553 Å for TPMCl, and 2.558 Å for TPMBr. Accordingly, the dihedral angles between these rings also vary, as summarized in Figure S29 and Table S8 (Supporting

© 2021 The Authors. Advanced Materials published by Wiley-VCH GmbH

Information). It has been reported that weak intramolecular interactions contribute to stabilizing the excited singlet and triplet states by reducing molecular vibrations or rotations.[6,40] As shown in Figure S30 (Supporting Information), the intermolecular interactions are changing by halogen atom substitution. The intermolecular distance between the hydrogen atom from the *N*-phenyl ring and the nitrogen of the imidazole ring is ≈3 Å for TPMN and TPMF, to 2.6 Å for TPMCl, TPMBr, and TPMI. The differences in electron-withdrawing ability and weak intramolecular interactions are expected to contribute to the variation in Φ_P for the TPMX series. For the fluorine and chlorine substituted emitters TPMF and TPMCl, the photophysical properties are affected by combined effects mainly from their electron-withdrawing ability and weak intramolecular interactions.

The subtle effect introduced by halogen atoms in the TPMX series was further confirmed by DFT simulations. As shown in Figures S21 and S22 (Supporting Information), the effect introduced by halogen atoms was barely observable for the SOC factor, while a clear difference for NTOs was observed for TPMBr and TPMI. This is consistent with the experimental results indicating that the heavy atom effect of bromine and iodine plays a more important role in the photophysical properties of TPMBr and TPMI than the intramolecular effects. An increased Φ_P and a decreased τ_P were obtained for TPMBr and TPMI. Such an effect has been widely used to boost URTP emissions from organic emitters.[18,41–43] However, since the halogen atom is quite far from the donor/acceptor of the emitter, the contribution of halogen atoms in NTOs is quite minor compared to that of URTP emitters with halogen atoms closer to the molecular core.[41]

2.4. Anti-Counterfeiting Device

Based on the fascinating emissive properties of these phenanthroimidazole derivatives, an anticounterfeiting device was demonstrated with a time-dependent Morse code feature. Emitters were diluted in the PMMA matrix and painted on a quartz substrate with a Morse code pattern, as shown in **Figure 5**, which was based on TPN without URTP properties, where TPMN exhibited the longest τ_P and TPMI exhibited the shortest τ_P. The device was further sealed with an oxygen barrier layer by drop casting of Exceval.[5,13] Under UV excitation, the Morse code represented the Arabic numeral "0," with fluorescence emission from the entire coating area. When the UV light was turned off, the URTP of TPMN and TPMI exhibited a Morse code pattern denoting the Arabic numeral "1." When the emission of TPMI vanished after cessation of the UV illumination because it has a shorter τ_P than TPMN, the phosphorescence emission of TPMN displayed a Morse code pattern representing the Arabic numeral "2." It is possible to fabricate more complicated patterns with time-dependent characteristics based on a combination of these materials. The group of purely organic phenanthroimidazole derivatives developed in this work demonstrates an excellent application potential in data encryption, with the advantages of fast synthesis and high product yield.

3. Conclusion

It was found that the substitution of a hydrogen atom of the imidazole ring by an *N*-phenyl ring can convert a purely organic emitter without phosphorescence into an efficient phosphorescent material at room temperature. By combining systematic photophysical studies, excited states dynamic simulations, kinetic modeling, and single-crystal structure analysis, we demonstrated that the presence of the *N*-phenyl group can alleviate the intrinsic non-radiative losses in the molecular structure, either from the singlet state, the triplet state, or both. The *N*-phenyl group with weak intramolecular interactions restricts out-of-plane motions in the excited state with respect to the hydrogen atom in TPN, giving rise to a higher

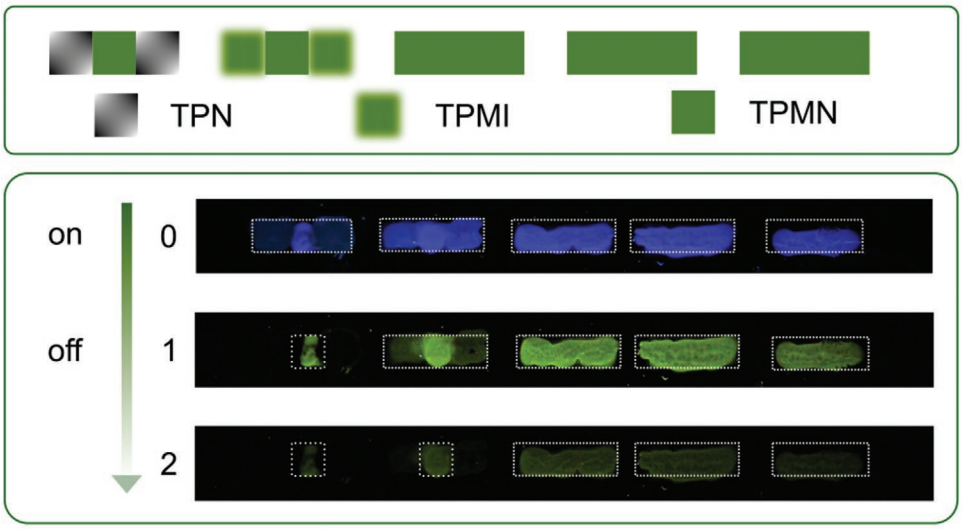

Figure 5. Data safety demonstration. An anticounterfeiting tag is fabricated with a combination of TPN, TPMN, and TPMI. The numbers 0, 1, 2 are Arabic numerals represented by the time-dependent Morse code.

© 2021 The Authors. Advanced Materials published by Wiley-VCH GmbH

photoluminescence quantum yield for both fluorescence and phosphorescence. A new method to realize URTP from non-phosphorescence emissive materials by suppressing intrinsic non-radiative losses was unveiled.

Further modifying the *N*-phenyl group with halogen atoms had subtle effects on the URTP properties. In addition to the widely investigated heavy atom effect in bromine- or iodine-substituted compounds, modification of the electron-withdrawing ability and intramolecular weak contacts plays a more important role in fluorinated or chlorinated derivatives. Based on these materials, an anti-counterfeiting device was fabricated with time-dependent Morse code patterns for data safety applications. We anticipate that this study will expand the molecular systems with URTP emission, enhance the understanding of the URTP mechanism down to the molecular level, and facilitate further investigation of URTP materials.

4. Experimental Section

Synthesis and Material Characterization: The synthesis details and ^{1}H NMR and MS results of TPN, TPMN, TPMF, TPMCl, TPMBr, and TPMI can be found in the Supporting Information. All emitter materials were purified by gradient zone sublimation before luminescence characterization.

Film Preparation: PMMA was dissolved in toluene at a concentration of 40 mg mL^{-1}, while TPMX was dissolved in toluene and TPN was dissolved in THF at concentrations of 10 mg mL^{-1}. Different blends were prepared by mixing PMMA and organic materials to obtain a mixed solvent with an emitter concentration of 2 wt% in the PMMA matrix. These blended films were then prepared by spin-coating onto cleaned and oxygen plasma-treated quartz substrates.

Photophysical Measurements: The steady-state PL spectra in DCM solutions were measured with a Spex FluoroMax spectrofluorometer, while UV–Vis absorption was obtained in DCM with a Shimadzu MPC 3100. The PLQY of these films was measured by a calibrated integrating sphere with a spectrometer (CAS 140 CT, Instrument Systems) and a UV-LED (340 nm, Thorlabs). To obtain the absolute values of Φ_F and Φ_P PLQY measurements were performed in either ambient nitrogen ($\Phi_F + \Phi_P$) or air (Φ_F) according to de Mello's method.[44,45] The steady-state fluorescence spectra of the emitters doped in PMMA films were collected during PLQY measurements in air. The phosphorescence spectra and time-resolved phosphorescence intensity were obtained by means of a custom-made setup in a nitrogen atmosphere with a UV-LED (365 nm, Thorlabs). The time-resolved phosphorescence intensity of a complete duty cycle was measured by a silicon photodetector (PDA100A, Thorlabs) under UV pulses (waveform generator: Keysight Agilent Technologies 8114A) in a nitrogen atmosphere. Phosphorescence spectra were obtained with a spectrometer orthogonally mounted along the excitation light path. The transient fluorescence measurements were carried out on two different setups. The fluorescence decay was measured by the time-correlated single-photon-counting (TCSPC) technique with a laser at 373 nm in air. Photons were detected by a photomultiplier tube (PicoQuant PMA Hybrid). To measure the time-resolved spectrum of TPN at 10 K and 50 K, a C5680 Hamamatsu streak camera system with a single sweep module (M5677) was utilized. The samples were excited at 400 nm with the frequency-doubled output from a Ti-sapphire laser (Coherent, Astrella, 5 mJ, 800 nm, 1 kHz). The sample was mounted in a closed-cycle helium cryostat (Advanced Research Systems). A 420 nm longpass filter was used to block the excitation light from entering the detector.

Molecular Simulation: All geometry optimization and excited-state calculations were performed by DFT at the cam-B3LYP/6-311g(d,p) (for C, H, O, N, F, Cl atoms) + LANL2DZdp (for Br, I atoms, with LANL2DZ ECP) level using the Gaussian16 package.[46–48] To simulate the experimental environment, all the excited-state calculations were combined with the state-specific polarizable continuum model (PCM),[49,50] where n-hexane was used as the solvent. The corresponding spin–orbit coupling parameters were evaluated by the PySOC program.[51]

Anticounterfeiting Device Fabrication: TPN was mixed in a PMMA matrix at a concentration of 6 wt%, while TPMN and TPMI were prepared at a concentration of 2 wt% in PMMA. The concentration of PMMA was 50 mg mL^{-1} in toluene. The quartz substrate was cleaned by ethanol and treated by oxygen plasma for 10 min. Solutions were painted on the substrate with a pipette, with a square area for the Morse code of ≈0.5 cm. After drying for 30 min in a fume hood, the substrate was sealed with an oxygen barrier layer Exceval (Kuraray Europe GmbH) and dried overnight.

Supporting Information

Supporting Information is available from the Wiley Online Library or from the author.

Acknowledgements

Y.L. is grateful for financial support from the China Scholarship Council (No. 201506160049) and the Graduate Academy of TU Dresden. L.J. acknowledges financial support from the China Scholarship Council (No. 201706375057). This project was supported by the National Natural Science Foundation of China (21506258, 21875286). This project received funding from the European Research Council (ERC) under the European Union's Horizon 2020 Research and Innovation Program (grant agreement no. 679213 "BILUM"). The authors thank Max Gmelch for his assistance in taking the URTP photographs shown in Figure 1b.

Open access funding enabled and organized by Projekt DEAL.

Note: The affiliations were corrected and the order updated on October 1, 2021, after initial publication online. One of the grant numbers in the acknowledgements section was also revised.

Conflict of Interest

The authors declare no conflict of interest.

Data Availability Statement

The data that support the findings of this study are available from the corresponding author upon reasonable request.

Keywords

non-radiative loss, phenanthroimidazole, room-temperature phosphorescence, triplet emission

Received: March 8, 2021
Revised: May 18, 2021
Published online: August 8, 2021

[1] M. A. Baldo, M. E. Thompson, S. R. Forrest, *Nature* **2000**, *403*, 750.
[2] M. Thompson, *MRS Bull.* **2007**, *32*, 694.
[3] D. Di, A. S. Romanov, L. Yang, J. M. Richter, J. P. H. Rivett, S. Jones, T. H. Thomas, M. A. Jalebi, R. H. Friend, M. Linnolahti, M. Bochmann, D. Credgington, *Science* **2017**, *356*, 159.
[4] S. Reineke, M. Thomschke, B. Lüssem, K. Leo, *Rev. Mod. Phys.* **2013**, *85*, 1245.

© 2021 The Authors. Advanced Materials published by Wiley-VCH GmbH

[5] M. Louis, H. Thomas, M. Gmelch, A. Haft, F. Fries, S. Reineke, *Adv. Mater.* **2019**, *31*, 1807887.
[6] Z. An, C. Zheng, Y. Tao, R. Chen, H. Shi, T. Chen, Z. Wang, H. Li, R. Deng, X. Liu, W. Huang, *Nat. Mater.* **2015**, *14*, 685.
[7] K. Jinnai, R. Kabe, C. Adachi, *Adv. Mater.* **2018**, *30*, 1800365.
[8] R. Kabe, N. Notsuka, K. Yoshida, C. Adachi, *Adv. Mater.* **2016**, *28*, 655.
[9] H. Thomas, D. L. Pastoetter, M. Gmelch, T. Achenbach, A. Schlögl, M. Louis, X. Feng, S. Reineke, *Adv. Mater.* **2020**, *32*, 2000880.
[10] M. Louis, H. Thomas, M. Gmelch, F. Fries, A. Haft, J. Lindenthal, S. Reineke, *Adv. Opt. Mater.* **2020**, *8*, 2000427.
[11] L. Gu, H. Shi, L. Bian, M. Gu, K. Ling, X. Wang, H. Ma, S. Cai, W. Ning, L. Fu, H. Wang, S. Wang, Y. Gao, W. Yao, F. Huo, Y. Tao, Z. An, X. Liu, W. Huang, *Nat. Photonics* **2019**, *13*, 406.
[12] G. Zhang, G. M. Palmer, M. W. Dewhirst, C. L. Fraser, *Nat. Mater.* **2009**, *8*, 747.
[13] M. Gmelch, H. Thomas, F. Fries, S. Reineke, *Sci. Adv.* **2019**, *5*, eaau7310.
[14] S. Hirata, *Adv. Opt. Mater.* **2017**, *5*, 1700116.
[15] K. Schmidt, S. Brovelli, V. Coropceanu, D. Beljonne, J. Cornil, C. Bazzini, T. Caronna, R. Tubino, F. Meinardi, Z. Shuai, J. L. Brédas, *J. Phys. Chem. A* **2007**, *111*, 10490.
[16] N. Gan, H. Shi, Z. An, W. Huang, *Adv. Funct. Mater.* **2018**, *28*, 1802657.
[17] R. Kabe, C. Adachi, *Nature* **2017**, *550*, 384.
[18] O. Bolton, K. Lee, H. J. Kim, K. Y. Lin, J. Kim, *Nat. Chem.* **2011**, *3*, 205.
[19] J. Wang, C. Wang, Y. Gong, Q. Liao, M. Han, T. Jiang, Q. Dang, Y. Li, Q. Li, Z. Li, *Angew. Chem., Int. Ed.* **2018**, *57*, 16821.
[20] Y. Tao, R. Chen, H. Li, J. Yuan, Y. Wan, H. Jiang, C. Chen, Y. Si, C. Zheng, B. Yang, G. Xing, W. Huang, *Adv. Mater.* **2018**, *30*, 1803856.
[21] M. A. El-Sayed, *J. Chem. Phys.* **1963**, *38*, 2834.
[22] Y. Xie, Y. Ge, Q. Peng, C. Li, Q. Li, Z. Li, *Adv. Mater.* **2017**, 29, 1606829.
[23] S. Hirata, K. Totani, J. Zhang, T. Yamashita, H. Kaji, S. R. Marder, T. Watanabe, C. Adachi, *Adv. Funct. Mater.* **2013**, *23*, 3386.
[24] F. Fries, M. Louis, R. Scholz, M. Gmelch, H. Thomas, A. Haft, S. Reineke, *J. Phys. Chem. A* **2020**, *124*, 479.
[25] K. Wang, F. Zhao, C. Wang, S. Chen, D. Chen, H. Zhang, Y. Liu, D. Ma, Y. Wang, *Adv. Funct. Mater.* **2013**, *23*, 2672.
[26] J. Drechsel, A. Petrich, M. Koch, S. Pfützner, R. Meerheim, S. Scholz, J. Drechsel, K. Walzer, M. Pfeiffer, K. Leo, *SID Int. Symp. Dig. Tech. Pap.* **2006**, *37*, 1692.
[27] H. Uoyama, K. Goushi, K. Shizu, H. Nomura, C. Adachi, *Nature* **2012**, *492*, 234.
[28] Y. Li, Q. Wei, L. Cao, F. Fries, M. Cucchi, Z. Wu, R. Scholz, S. Lenk, B. Voit, Z. Ge, S. Reineke, *Front. Chem.* **2019**, *7*, 688.
[29] F. B. Dias, T. J. Penfold, A. P. Monkman, *Methods Appl. Fluoresc.* **2017**, *5*, 012001.
[30] R. Scholz, P. Kleine, R. Lygaitis, L. Popp, S. Lenk, M. K. Etherington, A. P. Monkman, S. Reineke, *J. Phys. Chem. A* **2020**, *124*, 1535.
[31] S. J. Strickler, R. A. Berg, *J. Chem. Phys.* **1962**, *37*, 814.
[32] K. Narushima, Y. Kiyota, T. Mori, S. Hirata, M. Vacha, *Adv. Mater.* **2019**, *31*, 1807268.
[33] I. Rörich, A.-K. Schönbein, D. K. Mangalore, A. Halda Ribeiro, C. Kasparek, C. Bauer, N. I. Crăciun, P. W. M. Blom, C. Ramanan, *J. Mater. Chem. C* **2018**, *6*, 10569.
[34] H. Ma, Q. Peng, Z. An, W. Huang, Z. Shuai, *J. Am. Chem. Soc.* **2019**, *141*, 1010.
[35] Q. Zhang, H. Kuwabara, W. J. Potscavage, S. Huang, Y. Hatae, T. Shibata, C. Adachi, *J. Am. Chem. Soc.* **2014**, *136*, 18070.
[36] Q. Peng, Y. Yi, Z. Shuai, J. Shao, *J. Am. Chem. Soc.* **2007**, *129*, 9333.
[37] S. Yin, Q. Peng, Z. Shuai, W. Fang, Y. H. Wang, Y. Luo, *Phys. Rev. B: Condens. Matter Mater. Phys.* **2006**, *73*, 205409.
[38] J. Mei, N. L. C. Leung, R. T. K. Kwok, J. W. Y. Lam, B. Z. Tang, *Chem. Rev.* **2015**, *115*, 11718.
[39] S. Reineke, N. Seidler, S. R. Yost, F. Prins, W. A. Tisdale, M. A. Baldo, *Appl. Phys. Lett.* **2013**, *103*, 093302.
[40] J. Yang, X. Zhen, B. Wang, X. Gao, Z. Ren, J. Wang, Y. Xie, J. Li, Q. Peng, K. Pu, Z. Li, *Nat. Commun.* **2018**, *9*, 840.
[41] J. Wang, X. Gu, H. Ma, Q. Peng, X. Huang, X. Zheng, S. H. P. Sung, G. Shan, J. W. Y. Lam, Z. Shuai, B. Z. Tang, *Nat. Commun.* **2018**, *9*, 2963.
[42] X.-F. Wang, H.-Y. Xiao, P.-Z. Chen, Q.-Z. Yang, B. Chen, C.-H. Tung, Y.-Z. Chen, L.-Z. Wu, *J. Am. Chem. Soc.* **2019**, *141*, 5045.
[43] S. Reineke, M. A. Baldo, *Sci. Rep.* **2015**, *4*, 3797.
[44] J. C. de Mello, H. F. Wittmann, R. H. Friend, *Adv. Mater.* **1997**, *9*, 230.
[45] F. Fries, S. Reineke, *Sci. Rep.* **2019**, *9*, 15638.
[46] W. R. Wadt, P. J. Hay, *J. Chem. Phys.* **1985**, *82*, 284.
[47] T. Yanai, D. P. Tew, N. C. Handy, *Chem. Phys. Lett.* **2004**, *393*, 51.
[48] R. Krishnan, J. S. Binkley, R. Seeger, J. A. Pople, *J. Chem. Phys.* **1980**, *72*, 650.
[49] R. Improta, G. Scalmani, M. J. Frisch, V. Barone, *J. Chem. Phys.* **2007**, *127*, 074504.
[50] R. Improta, V. Barone, G. Scalmani, M. J. Frisch, *J. Chem. Phys.* **2006**, *125*, 054103.
[51] X. Gao, S. Bai, D. Fazzi, T. Niehaus, M. Barbatti, W. Thiel, *J. Chem. Theory Comput.* **2017**, *13*, 515.

© 2021 The Authors. Advanced Materials published by Wiley-VCH GmbH